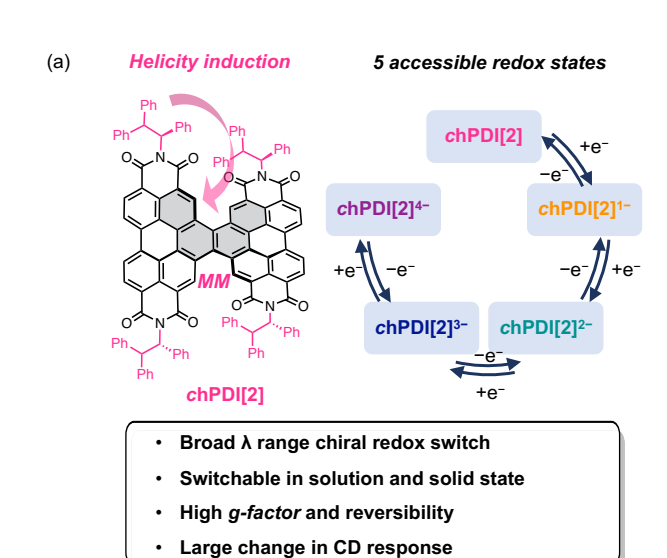
# **Near-Infrared, Organic Chiroptic Switch with High Dissymmetry Factors**

Si Tong Bao,<sup>†</sup> Shayan Louie,<sup>†</sup> Haoyu Jiang,<sup>†</sup> Qifeng Jiang,<sup>†</sup> Shantao Sun,<sup>†</sup> Michael L. Steigerwald,<sup>†</sup> Colin Nuckolls\*,<sup>†</sup>, Zexin Jin\*,<sup>‡</sup>,§

**ABSTRACT:** Here we unveil a chiral molecular redox switch derived from PDI-based twistacenes—chPDI[2] that has the remarkable attributes of high-intensity and broad-band chiral response. This material exhibits facile, stable, and reversible multistate chiroptical switching behavior over a broad active wavelength range close to 700 nm, encompassing ultraviolet, visible, and near-infrared regions. Upon reduction, chPDI[2] exhibits a substantial increase in the amplitude of its circular dichroic response, with an outstanding  $|\Delta\Delta\varepsilon| > 300 \text{ M}^{-1} \text{ cm}^{-1}$  and a high dissymmetry factor of  $3 \times 10^{-2}$  at 960 nm. DFT calculations suggest that the long wavelength CD signal for doubly reduced chPDI[2] originates from the excitation of the PDI backbone to the  $\pi^*$  orbital of the bridging alkene. Importantly, the dimer's molecular contortion facilitates ionic diffusion, enabling chiral switching in solid state films. The high dissymmetry factors and near-infrared response establish chPDI[2] as a unique chiroptic switch.

Growing interest in organic optoelectronics has incentivized the development of chiroptical switches responsive to external stimuli such as light, <sup>1-8</sup> pH, <sup>9-12</sup> and electric potential. <sup>13-18</sup> These chiroptical switches offer new prospects in molecular information processing and storage, <sup>19,20</sup> high sensitivity detection of various analytes, <sup>21,22</sup> and switchable stereoselectivity in asymmetric catalysis. <sup>23-25</sup> However, designing chiroptical switches that exhibit both a high chiroptical response to stimulus and a broad active wavelength range poses a significant challenge. Furthermore, only a few examples have demonstrated that switchable behavior is retained in the solid state, which is essential for materials applications. <sup>6,14,18,26,27</sup>

We recently reported a new type of dynamic, axial chirality in perylene diimide (PDI)-based twistacenes, 28-30 where remote chiral substituents on the imide position control the helicity of the aromatic core. Here, we describe the chiroptical switching of a new chPDI[2] derivative by manipulating the multiple redox states of the PDI subunits (Figure 1a). Adorned with bulky chiral triphenylethyl side chains, the chPDI[2] chiroptic switch exhibits a high  $|g_{abs}|$  of  $1.2 \times 10^{-2}$  in solution. Upon reduction, the reduced species show circular dichroism (CD) signal changes with exceptionally high chiroptical response ( $|\Delta \Delta \varepsilon|$  > 300 M<sup>-1</sup> cm<sup>-1</sup>) and dissymmetry factors,  $|g_{abs}|$  (as high as 3 × 10<sup>-2</sup>). Moreover, these switching events occur over broad wavelength ranges, extending beyond NIR wavelengths (>900 nm). The magnitude of the redox-driven chiroptical modulation, along with the molecule's extensive switchable wavelength range, are among the highest observed in redox switchable molecules (Figure 1b). Enhanced ionic diffusion facilitated by molecular contortion allows stable and robust redox switching in both solution and solid state. Importantly, the high  $|g_{abs}|$  is intrinsic to the molecular system and not a consequence of aggregation. These results chart a clear path for chiroptic valves that operate at NIR wavelengths.



(b) 300 chPDI[2] (This work) Maximum |ΔΔε| (L M<sup>-1</sup>cm<sup>-1</sup>) 00 00  $|\Delta\Delta\varepsilon| = 320 \text{ M}^{-1} \text{ cm}^{-1}$ A (Canary 2000) B (Crassous 2021) C (Crassous 2010) D (Teplý 2014) F (Suzuki 2001) F (Suzuki 2009) G (Diederich 2014) I (Suzuki 2016) H (Crassous 2012) 150 300 450 600 750 1050 900 λ (nm)

<sup>&</sup>lt;sup>†</sup>Department of Chemistry, Columbia University, New York, New York 10027, United States

<sup>&</sup>lt;sup>‡</sup>Research Center for Industries of the Future, Westlake University, Hangzhou, Zhejiang 310030, China

<sup>§</sup>School of Engineering, Westlake University, Hangzhou, Zhejiang 310030, China.

**Figure 1**. (a) Structure of *chPDI*[2], whose chiroptical signal can be tuned via access to each of its 5 redox states. (b) Comparison of the maximum  $|\Delta\Delta\epsilon|$  and active wavelength range of *chPDI*[2] with other redox-tunable, chiral small molecules. Systems compared include derivatives of metallamethionine (A<sup>31</sup>), metallahelicene (B,<sup>32</sup> C,<sup>33</sup> H<sup>34</sup>), helicene (D,<sup>35</sup> E,<sup>36</sup> F,<sup>37</sup> G<sup>38</sup>), and biphenyl (I<sup>39</sup>). See Figure S1 and Table S1-S3 for detailed information on the structures and properties of compared systems.

We synthesized *chPDI*[2] by treating helical perylene tetracarboxylic dianhydride[2] with (S)-1,2,2-triphenylethylamine (Scheme S1). This derivative with the bulky substituents has the largest helicity induction effect we observed. 28 chPDI[2] exhibits an outstanding  $|\Delta\varepsilon|$  of 340 M<sup>-1</sup> cm<sup>-1</sup> and chiral dissymmetry factor  $|g_{abs}|$  of  $1.2 \times 10^{-2}$  at 471 nm in THF (Figure 3a, pink trace). Geometry optimization calculation reveals a nearly exclusive chirality induction effect in the triphenyl-substituted chPDI[2] (Figure S2).<sup>28</sup> In cyclic voltammetry (CV) and differential pulse voltammetry (DPV) of chPDI[2], we observed four consecutive reversible single-electron reduction steps for chPDI[2] at half-wave potentials of -0.89, -1.04, -1.50 and -1.68 V vs the ferrocene/ferrocenium couple (Fc/Fc<sup>+</sup>) (Figure S3). Each of these five redox states exhibits a visible color change, corresponding to the four accessible reduced states of chPDI[2]. These results indicate that the five states can be reversibly accessed via an electrochemical process.

We next highlight the important finding that *chPDI*[2] can operate as a solid state chiroptical redox switch. We hypothesized that the dimer's molecular contortion facilitates the ion diffusion, ensuring charge balance in the solid state.<sup>40</sup> To test this theory, we alternated between the reduction and oxidation of the molecule by cycling between different voltage potentials (Figure 2a). Thin films of *chPDI*[2] were prepared by spin coating chloroform solutions onto an ITO coated glass slide. The slide was then assembled into a three-electrode setup in a 0.1 M solution of KCl (Figure S4).

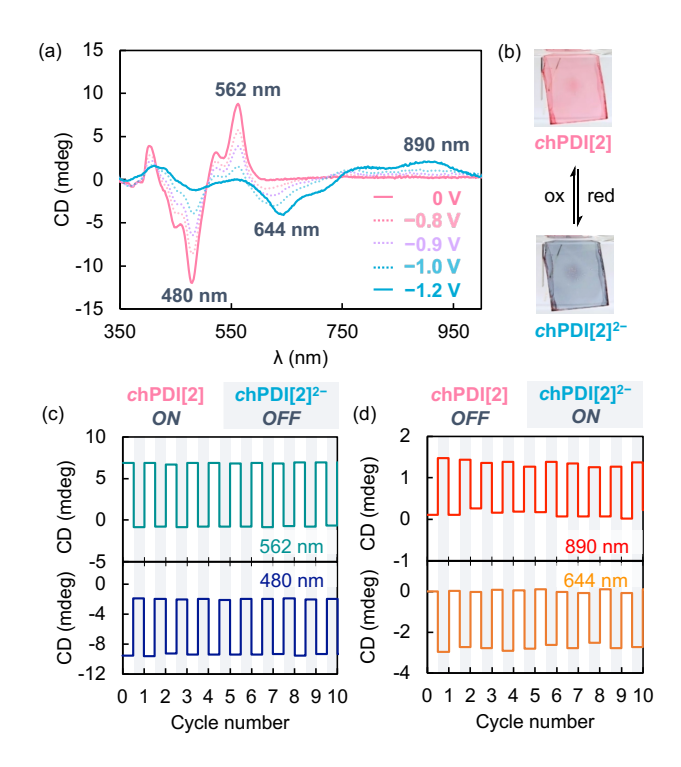


**Figure 2.** (a) CD spectra of the electrochemical switching of *chPDI*[2] in the solid state. CV and UV are shown in Figures S5-S6. All voltages reported are referenced to Ag/AgCl. (b) Film color change between *chPDI*[2] and *chPDI*[2]<sup>2-</sup> on a 2.5 × 2.5 cm ITO coated glass slide. c) and d) Cycling stability of *chPDI*[2] switch at 890 nm (red), 644 nm (orange), 562 nm (green) and 480 nm (blue).

The films underwent step-wise reduction with progressively more negative voltage potentials. In the neutral state, chPDI[2] film exhibits two bands of chiroptical signals (Figure 2a): 420 nm to 510 nm (negative Cotton effect peaks at 480 nm) and 510 nm to 590 nm (positive Cotton effect peaks at 562 nm). Applying a voltage at -1.2 V (vs. Ag/AgCl) caused the CD signals of the film to change drastically. Both bands from the neutral chPDI[2] disappeared, replaced by a new negative signal at 644 nm and a broad positive NIR CD response at 890 nm. The film changed color from pink to green, then to blue (Figure 2b and Supporting Information Video). These changes align with further studies in the solution state (vide infra) and are attributed to the reduction of chPDI[2] to chPDI[2]<sup>2-</sup>. Further reduction of chPDI[2] was prohibited due to the limited voltage window of the aqueous electrolyte. 40 This finding creates the possibility of incorporating these molecules into solid state devices.

The chPDI[2] films showed excellent reversibility in switching between the neutral and the reduced state over many cycles (Figure 2c). This robust switch allowed significant modulation of chiral signals spanning an impressively wide range of nearly 700 nm. Depending on the wavelength window, chPDI[2] film forms two distinct binary switching modes. At 480 nm and 562 nm, chPDI[2] serves as an "ON-OFF" switch, exhibiting active CD signals in the neutral state which can be turned "OFF" upon reduction to chPDI[2]<sup>2-</sup>. Conversely, at 640 nm and 890 nm, the molecule behaves as an "OFF-ON" switch, appearing CD silent in the neutral state but can be turned "ON" upon reduction. These results, taken together, demonstrate that chPDI[2]

can function as a solid state redox chiral switch with intense chiroptical response in the NIR region and great stability.

We next describe the chiroptical properties of all four reduced states in solution. To avoid aggregation, a low concentration  $(10^{-6}\,\mathrm{M})$  of chPDI[2] in THF was subject to titration using decamethylcobaltocene (CoCp2\*) or lithium diisopropylamide (LDA). Chemical reduction was successful only in THF and DMF, presumably due to the stabilization provided by higher polarity solvents. The anions were well-characterized by UV-vis, CD, and electron paramagnetic resonance (EPR) spectroscopy.

The addition of 1 equivalent of CoCp<sub>2</sub>\* to a pink *chPDI*[2] solution led to the formation of a pale-yellow *chPDI*[2]<sup>1-</sup> solution. The emergence of monoanionic species is supported by the strong EPR signal with a g-value of 2.003, suggesting the presence of organic radicals (Figure S7). A bathochromic shift was observed in the UV-vis spectrum, where broad peaks appeared from 640 to 910 nm, along with a new broad band centered at 1600 nm (Figure 3a, orange trace). In the CD spectra of *chPDI*[2]<sup>1-</sup>, a new negative signal emerged at 600 nm, along with a broad positive NIR CD response between 680 and 900 nm (Figure 3b, orange trace).

Adding 2 equivalents of  $CoCp_2^*$  generated a light blue solution of  $chPDI[2]^{2^-}$  (Figure 3a) with a negligible EPR signal (Figure S7). Simulated singlet state spectrum of  $chPDI[2]^{2^-}$  shows better overlap with the experimental spectra than the simulated triplet state spectrum. Considering both simulated and experimental results, we assigned the dianion as a singlet state (Figure S17). In the UV-vis spectrum, a notable growth of the broad peak centered at 1600 nm emerged. In the CD spectrum,  $|\Delta \Delta \varepsilon_{47Inm}|$  between the neutral and reduced state rose to an impressive 321  $M^{-1}$  cm<sup>-1</sup> (Table S2). This drastic change in  $\Delta \varepsilon$  value is among the highest observed in redox switchable

organic small molecules (Table S3). Furthermore,  $chPDI[2]^{2^{-}}$  also exhibits a new positive NIR peak at 960 nm with a  $|\Delta\varepsilon|$  of 57 M<sup>-1</sup> cm<sup>-1</sup> and a  $|g_{abs}|$  value of 0.03 (Figure S8).<sup>43</sup> This response in the NIR region is rarely reported among organic chiral small molecules<sup>34,44–46</sup> and suggests potential application of the molecule in biological sensing<sup>47,48</sup> and optical communication.<sup>42</sup>

An excess of CoCp2\* produced a dark blue solution of chPDI[2]<sup>3-</sup>, which exhibits a broad EPR signal with a g-value of 2.003 (Figure S7). In the UV-vis spectrum, the broad band at 1600 nm disappeared (Figure 3a), while the CD signal at 630 nm and 960 nm underwent a decrease in intensity (Figure 3b). Finally, the fully reduced chPDI[2]<sup>4-</sup> was realized using an excess of LDA (Figure 3a and Figure S9) or sodium naphthalene (Figure S10).<sup>49</sup> The UV-vis spectrum displayed a new peak appearing at 550 nm while all NIR absorption above 850 nm completely vanished. The 4<sup>-</sup> state appears EPR silent (Figure S7), consistent with its diamagnetic nature. In the CD spectrum, a new positive response emerged at 560 nm, accompanied by a negative signal at 640 nm. Oxidation of chPDI[2]<sup>4-</sup> to the neutral chPDI[2] was achieved through the addition of one drop of 2M HCl to the solution (Figure S11), verifying the reversibility of the redox process.

Similar redox behavior can also be achieved electrochemically (Figures S12-S13). Spectroelectrochemistry demonstrates that multi-state chiroptical redox switching of *chPDI*[2] takes place in the solution state over a wide range of wavelengths, from the visible range to the NIR range and is reversible. The electrochemical switching of this material allows it to function as a chiroptic switch that can serve as either a binary or trinary switch at five wavelengths (Figure S14).

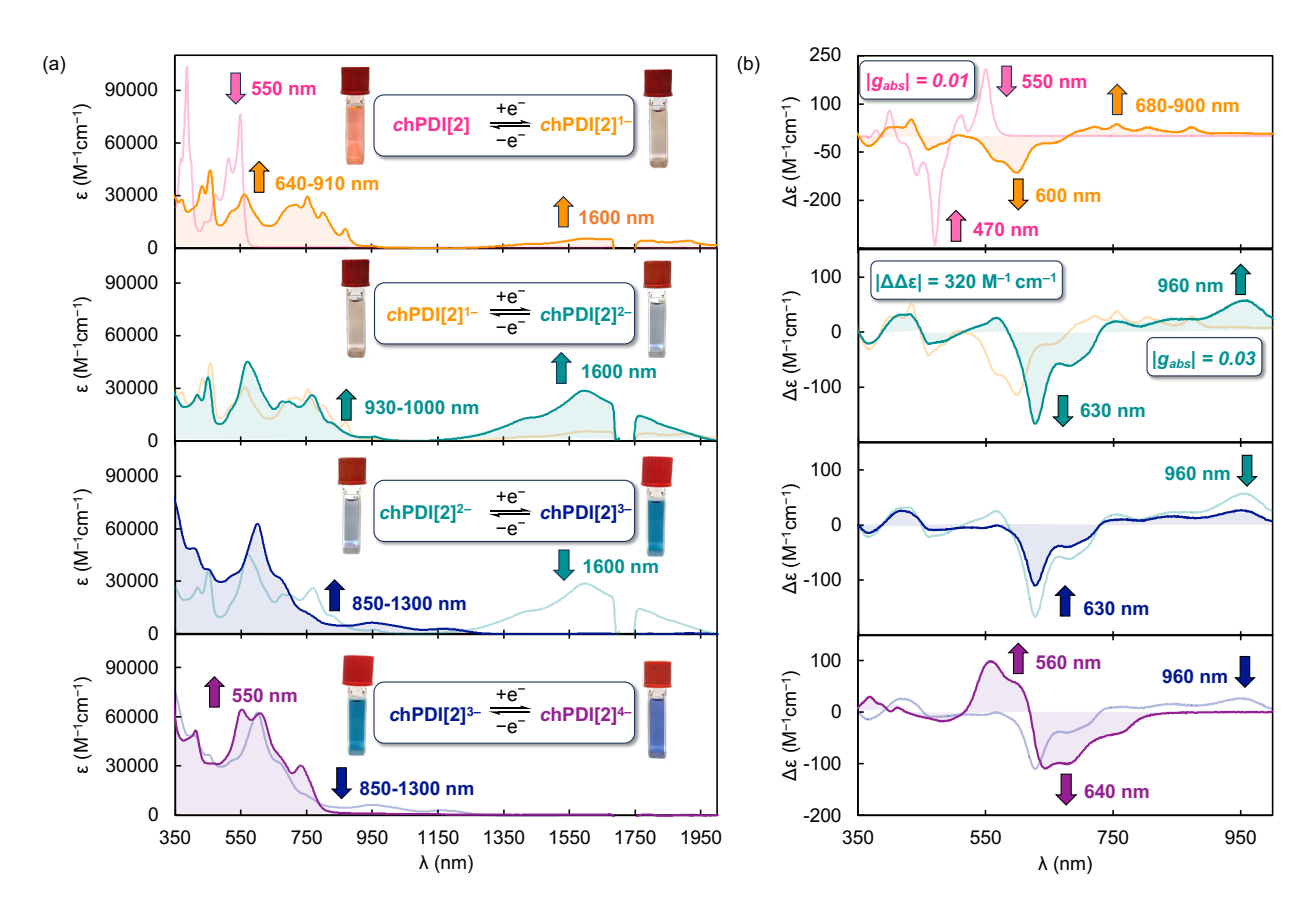


**Figure 3.** (a) UV-vis and (b) CD spectra of *chPDI*[2] (pink), *chPDI*[2]<sup>1-</sup> (orange), *chPDI*[2]<sup>2-</sup> (green), *chPDI*[2]<sup>3-</sup>(blue), and *chPDI*[2]<sup>4-</sup> (purple) in THF.

To explore the origin of the chiroptical changes in the reduced states of chPDI[2], we performed density functional theory (DFT) calculations on chPDI[2] and all four reduced species. Model compound MM-chPDI[2]-Me with methyl substituents on the imides were used to simplify the calculations (Figure 4), and all the geometries were optimized at B3LYP/6-31+G(d) level of theory. As shown in Table S4, the dihedral angles between PDI units increase marginally with higher reduction states, suggesting that changes in the CD signal originate primarily from changes in molecular electronics rather than molecular geometry. Time-dependent density-functional theory (TD-DFT) simulations at the CAM-B3LYP/6-31+G(d) level of theory correlate well with the experimental results (Figures S15-16), indicating the helicity of [4]helicene subunits stay persistent under reduction. Figure 4a compares the simulated CD spectra and electronic transition states of MM-chPDI[2]-Me and its 2<sup>-</sup> state. Natural transition orbital (NTO) analysis<sup>50</sup> visualized the main contributing transitions between two molecular orbitals (Figure 4b). The lowest-energy transition  $(S_0 \rightarrow S_1)$ of neutral MM-chPDI[2]-Me is mainly attributed to the excitation from the PDI backbone's HOMO to LUMO. On the other hand, the  $2^-$  state's NIR transition ( $S_0 \rightarrow S_2$ ) originates from the excitation of the PDI backbone to the  $\pi^*$  orbital of the bridging alkene. Furthermore, by closely examining the electric and magnetic dipole moment vectors (Figures S25), we attribute the 2 state's high dissymmetry factor to the large magnetic dipole moment in the  $S_0 \rightarrow S_2$  transition (Table S7).<sup>51</sup> Interestingly, the

dipole moment vectors are along the conjugated backbone in the neutral state, while in 2<sup>-</sup> state the dipole moment vectors are orthogonal to the conjugated backbone (Figures S23 and S25). Lastly, the TD-DFT calculation suggests that the lowest-energy transition of the 2<sup>-</sup> state exhibits a CD response (Figure S19), suggesting the experimental absorption at 1600 nm of the 2<sup>-</sup> state may be CD active.

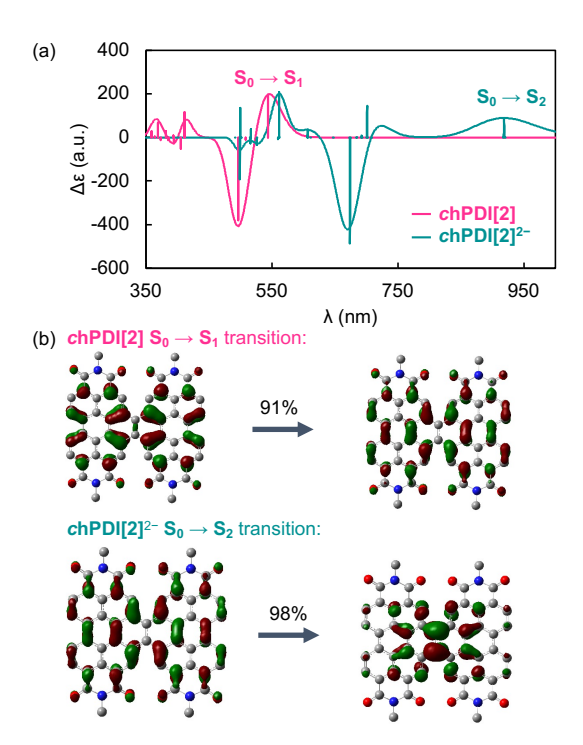


**Figure 4.** (a) Simulated CD spectra and transitions of *chPDI*[2] (pink) and *chPDI*[2]<sup>2-</sup> (green) at the CAM-B3LYP/6-31G(d) level of theory in the gas phase. Simulated spectra (Figures S15-16) are red-shifted according to the experimental UV-vis spectra. See Figures S18-S19 for full simulated spectra and transitions for all redox states of *chPDI*[2]. (b) NTO analysis of the lowest energy transition of *chPDI*[2] (544 nm) and the NIR transition of *chPDI*[2]<sup>2-</sup> (918 nm). The percentage number indicates the weight percentage of the dominant transition states of interest. The wavelength number is simulated by DFT. See Figures S20-S22 for detailed information.

In conclusion, *chPDI[2]* demonstrates a remarkable suite of properties as a chiroptic switch, making it useful for applications in molecular memory, asymmetric catalysis, and optoelectronics. UV-vis, CD, and EPR spectroscopy were used to characterize the various redox states of *chPDI[2]*, and DFT calculations were used to probe the origins of the optical transition. The material's wide active wavelength range, along with its enormous chiral response in the NIR region, positions it as a novel and valuable addition to the family of chiral redox switches. Finally, the switch's dual functionality in both solution and solid state films holds promise for future incorporation into devices.

### ASSOCIATED CONTENT

## **Supporting Information**

The Supporting Information is available free of charge on the ACS Publications website.

- Synthetic details and characterization, 1H NMR studies, 13C NMR studies, EPR studies, electrochemical data, and calculation details (PDF)
- Film color change between chPDI[2] and chPDI[2]<sup>2-</sup> on an ITO coated glass slide (MP4)

#### **AUTHOR INFORMATION**

## **Corresponding Author**

- \* jinzexin@westlake.edu.cn
- \* cn37@columbia.edu

### **ACKNOWLEDGMENT**

C.N. thanks Sheldon and Dorothea Buckler for their generous support. This research was supported by supported by the National Science Foundation under award number CHE-2304946. This material is also based upon work supported by the Defense Advanced Research Projects Agency (DARPA) under Agreement No. HR00112390109. Z. J. acknowledges funding from Research Center for Industries of the Future at Westlake University and Westlake Education Foundation. We thank the Precision Biomolecular Characterization Facility (PBCF) at Columbia University. The ECD spectra were recorded at the Precision Biomolecular Characterization Facility (PBCF) at Columbia University. Essential instrumentation in the PBCF was made possible by funding from the U.S. National Institutes of Health under award Award No. 1S10OD025102-01. We thank Westlake University HPC Center for computing support. We thank Dr. John Decatur (Columbia University) for his management of NMR facilities and Dr. Jerry Chang (Columbia University) for his management of the PBCF. We also thank Prof. Lauren Marbella (Columbia University) for access to the EPR spectrometer.

# **REFERENCES**

- (1) Koumura, N.; Zijlstra, R. W. J.; van Delden, R. A.; Harada, N.; Feringa, B. L. Light-Driven Monodirectional Molecular Rotor. *Nature* **1999**, *401* (6749), 152–155. https://doi.org/10.1038/43646.
- (2) Feringa, B. L.; van Delden, R. A.; Koumura, N.; Geertsema, E. M. Chiroptical Molecular Switches. *Chem. Rev.* **2000**, *100* (5), 1789–1816. https://doi.org/10.1021/cr9900228.
- (3) Isla, H.; Crassous, J. Helicene-Based Chiroptical Switches. *Comptes Rendus Chim.* **2016**, *19* (1), 39–49. https://doi.org/10.1016/j.crci.2015.06.014.
- (4) Wigglesworth, T. J.; Sud, D.; Norsten, T. B.; Lekhi, V. S.; Branda, N. R. Chiral Discrimination in Photochromic Helicenes. *J. Am. Chem. Soc.* **2005**, *127* (20), 7272–7273. https://doi.org/10.1021/ja050190j.
- (5) Tani, Y.; Ubukata, T.; Yokoyama, Y.; Yokoyama, Y. Chiral Helicenoid Diarylethene with Highly Diastereoselective Photocyclization <sup>1</sup>. *J. Org. Chem.* **2007**, *72* (5), 1639–1644. https://doi.org/10.1021/jo062022v.
- (6) Wang, Z. Y.; Todd, E. K.; Meng, X. S.; Gao, J. P. Dual Modulation of a Molecular Switch with Exceptional Chiroptical Properties. *J. Am. Chem. Soc.* **2005**, *127* (33), 11552–11553. https://doi.org/10.1021/ja0526721.
- (7) Zheng, Z.; Hu, H.; Zhang, Z.; Liu, B.; Li, M.; Qu, D.-H.; Tian, H.; Zhu, W.-H.; Feringa, B. L. Digital Photoprogramming of Liquid-Crystal Superstructures Featuring Intrinsic Chiral Photoswitches. *Nat. Photonics* **2022**, *16* (3), 226–234. https://doi.org/10.1038/s41566-022-00957-5.

- (8) Petermayer, C.; Dube, H. Circular Dichroism Photoswitching with a Twist: Axially Chiral Hemiindigo. *J. Am. Chem. Soc.* **2018**, *140* (42), 13558–13561. https://doi.org/10.1021/jacs.8b07839.
- (9) Anger, E.; Srebro, M.; Vanthuyne, N.; Roussel, C.; Toupet, L.; Autschbach, J.; Réau, R.; Crassous, J. Helicene-Grafted Vinyl- and Carbene-Osmium Complexes: An Example of Acid–Base Chiroptical Switching. *Chem. Commun.* **2014**, *50* (22), 2854–2856. https://doi.org/10.1039/C3CC47825D.
- (10) Saleh, N.; Moore II, B.; Srebro, M.; Vanthuyne, N.; Toupet, L.; Williams, J. A. G.; Roussel, C.; Deol, K. K.; Muller, G.; Autschbach, J.; Crassous, J. Acid/Base-Triggered Switching of Circularly Polarized Luminescence and Electronic Circular Dichroism in Organic and Organometallic Helicenes. *Chem. Eur. J.* **2015**, *21* (4), 1673–1681. https://doi.org/10.1002/chem.201405176.
- (11) Reyes-Gutiérrez, P. E.; Jirásek, M.; Severa, L.; Novotná, P.; Koval, D.; Sázelová, P.; Vávra, J.; Meyer, A.; Císařová, I.; Šaman, D.; Pohl, R.; Štěpánek, P.; Slavíček, P.; Coe, B. J.; Hájek, M.; Kašička, V.; Urbanová, M.; Teplý, F. Functional Helquats: Helical Cationic Dyes with Marked, Switchable Chiroptical Properties in the Visible Region. *Chem. Commun.* **2015**, *51* (9), 1583–1586. https://doi.org/10.1039/C4CC08967G.
- (12) Liang, H.; Hua, B.; Xu, F.; Gan, L.-S.; Shao, L.; Huang, F. Acid/Base-Tunable Unimolecular Chirality Switching of a Pillar[5]Azacrown Pseudo[1]Catenane. *J. Am. Chem. Soc.* **2020**, *142* (46), 19772–19778. https://doi.org/10.1021/jacs.0c10570.
- (13) Canary, J. W. Redox-Triggered Chiroptical Molecular Switches. *Chem. Soc. Rev.* **2009**, *38* (3), 747–756. https://doi.org/10.1039/B800412A.
- (14) Zheng, J.; Qiao, W.; Wan, X.; Gao, J. P.; Wang, Z. Y. Near-Infrared Electrochromic and Chiroptical Switching Materials: Design, Synthesis, and Characterization of Chiral Organogels Containing Stacked Naphthalene Diimide Chromophores. *Chem. Mater.* **2008**, *20* (19), 6163–6168. https://doi.org/10.1021/cm8014644.
- (15) Míšek, J.; Vargas Jentzsch, A.; Sakurai, S.; Emery, D.; Mareda, J.; Matile, S. A Chiral and Colorful Redox Switch: Enhanced  $\pi$  Acidity in Action. *Angew. Chem. Int. Ed.* **2010**, *49* (42), 7680–7683. https://doi.org/10.1002/anie.201003722.
- (16) Xiao, C.; Wu, W.; Liang, W.; Zhou, D.; Kanagaraj, K.; Cheng, G.; Su, D.; Zhong, Z.; Chruma, J. J.; Yang, C. Redox-Triggered Chirality Switching and Guest-Capture/Release with a Pillar[6]Arene-Based Molecular Universal Joint. *Angew. Chem. Int. Ed.* **2020**, *59* (21), 8094–8098. https://doi.org/10.1002/anie.201916285.
- (17) Ohta, E.; Sato, H.; Ando, S.; Kosaka, A.; Fukushima, T.; Hashizume, D.; Yamasaki, M.; Hasegawa, K.; Muraoka, A.; Ushiyama, H.; Yamashita, K.; Aida, T. Redox-Responsive Molecular Helices with Highly Condensed π-Clouds. *Nat. Chem.* **2011**, *3* (1), 68–73. https://doi.org/10.1038/nchem.900.
- (18) Wang, C.; Liu, L.; Wang, J.; Yan, Y. Electrochemically Switchable Circularly Polarized Photoluminescence within Self-Assembled Conducting Polymer Helical Microfibers. *J. Am. Chem. Soc.* **2022**, *144* (43), 19714–19718. https://doi.org/10.1021/jacs.2c10023.
- (19) Mammana, A.; D'Urso, A.; Lauceri, R.; Purrello, R. Switching Off and On the Supramolecular Chiral Memory in Porphyrin Assemblies. *J. Am. Chem. Soc.* **2007**, *129* (26), 8062–8063. https://doi.org/10.1021/ja071447b.
- (20) Dor, O. B.; Yochelis, S.; Mathew, S. P.; Naaman, R.; Paltiel, Y. A Chiral-Based Magnetic Memory Device without a Permanent Magnet. *Nat. Commun.* **2013**, *4* (1), 2256. https://doi.org/10.1038/ncomms3256. (21) Dai, Z.; Lee, J.; Zhang, W. Chiroptical Switches: Applications in Sensing and Catalysis. *Molecules* **2012**, *17* (2), 1247–1277. https://doi.org/10.3390/molecules17021247.
- (22) Formen, J. S. S. K.; Wolf, C. Chiroptical Switching and Quantitative Chirality Sensing with (Pseudo)Halogenated Quinones. *Angew. Chem. Int. Ed.* **2021**, *60* (52), 27031–27038. https://doi.org/10.1002/anie.202111542.
- (23) Ooi, T. Heat and Light Switch a Chiral Catalyst and Its Products. *Science* **2011**, *331* (6023), 1395–1396. https://doi.org/10.1126/science.1203272.
- (24) Wang, J.; Feringa, B. L. Dynamic Control of Chiral Space in a Catalytic Asymmetric Reaction Using a Molecular Motor. *Science*

- **2011**, *331* (6023), 1429–1432. https://doi.org/10.1126/science.1199844.
- (25) Stoll, R. S.; Peters, M. V.; Kuhn, A.; Heiles, S.; Goddard, R.; Bühl, M.; Thiele, C. M.; Hecht, S. Photoswitchable Catalysts: Correlating Structure and Conformational Dynamics with Reactivity by a Combined Experimental and Computational Approach. *J. Am. Chem. Soc.* **2009**, *131* (1), 357–367. https://doi.org/10.1021/ja807694s.
- (26) Zheng, Y.; Cui, J.; Zheng, J.; Wan, X. Near-Infrared Electro-chromic and Chiroptical Switching Polymers: Synthesis and Characterization of Helical Poly(N-Propargylamides) Carrying Anthraquinone Imide Moieties in Side Chains. *J. Mater. Chem.* **2010**, *20* (28), 5915–5922. https://doi.org/10.1039/B927360C.
- (27) Yang, G.; Yu, Y.; Yang, B.; Lu, T.; Cai, Y.; Yin, H.; Zhang, H.; Zhang, N.-N.; Li, L.; Zhang, Y.-M.; Zhang, S. X.-A. A Multiple Chirality Switching Device for Spatial Light Modulators. *Angew. Chem.* **2021**, *133* (4), 2046–2051. https://doi.org/10.1002/ange.202009916.
- (28) Bao, S. T.; Jiang, H.; Schaack, C.; Louie, S.; Steigerwald, M. L.; Nuckolls, C.; Jin, Z. Remote Control of Dynamic Twistacene Chirality. *J. Am. Chem. Soc.* **2022**, *144* (41), 18772–18777. https://doi.org/10.1021/jacs.2c08323.
- (29) Bao, S. T.; Jiang, H.; Jin, Z.; Nuckolls, C. Fusing Perylene Diimide with Helicenes. *Chirality* **2023**, *35* (10), 656–672. https://doi.org/10.1002/chir.23561.
- (30) Zhong, Y.; Kumar, B.; Oh, S.; Trinh, M. T.; Wu, Y.; Elbert, K.; Li, P.; Zhu, X.; Xiao, S.; Ng, F.; Steigerwald, M. L.; Nuckolls, C. Helical Ribbons for Molecular Electronics. *J. Am. Chem. Soc.* **2014**, *136* (22), 8122–8130. https://doi.org/10.1021/ja503533y.
- (31) Zahn, S.; Canary, J. W. Electron-Induced Inversion of Helical Chirality in Copper Complexes of N,N-Dialkylmethionines. *Science* **2000**, 288 (5470), 1404–1407. https://doi.org/10.1126/science.288.5470.1404.
- (32) Kos, M.; Rodríguez, R.; Storch, J.; Sýkora, J.; Caytan, E.; Cordier, M.; Císařová, I.; Vanthuyne, N.; Williams, J. A. G.; Žádný, J.; Církva, V.; Crassous, J. Enantioenriched Ruthenium-Tris-Bipyridine Complexes Bearing One Helical Bipyridine Ligand: Access to Fused Multihelicenic Systems and Chiroptical Redox Switches. *Inorg. Chem.* **2021**, *60* (16), 11838–11851. https://doi.org/10.1021/acs.inorg-chem.1c01379.
- (33) Norel, L.; Rudolph, M.; Vanthuyne, N.; Williams, J. A. G.; Lescop, C.; Roussel, C.; Autschbach, J.; Crassous, J.; Réau, R. Metallahelicenes: Easily Accessible Helicene Derivatives with Large and Tunable Chiroptical Properties. *Angew. Chem. Int. Ed.* **2010**, *49* (1), 99–102. https://doi.org/10.1002/anie.200905099.
- (34) Anger, E.; Srebro, M.; Vanthuyne, N.; Toupet, L.; Rigaut, S.; Roussel, C.; Autschbach, J.; Crassous, J.; Réau, R. Ruthenium-Vinylhelicenes: Remote Metal-Based Enhancement and Redox Switching of the Chiroptical Properties of a Helicene Core. *J. Am. Chem. Soc.* **2012**, *134* (38), 15628–15631. https://doi.org/10.1021/ja304424t.
- (35) Pospíšil, L.; Bednárová, L.; Štěpánek, P.; Slavíček, P.; Vávra, J.; Hromadová, M.; Dlouhá, H.; Tarábek, J.; Teplý, F. Intense Chiroptical Switching in a Dicationic Helicene-Like Derivative: Exploration of a Viologen-Type Redox Manifold of a Non-Racemic Helquat. *J. Am. Chem. Soc.* **2014**, *136* (31), 10826–10829. https://doi.org/10.1021/ja500220j.
- (36) Nishida, J.; Suzuki, T.; Ohkita, M.; Tsuji, T. A Redox Switch Based on Dihydro[5]Helicene: Drastic Chiroptical Response Induced by Reversible C–C Bond Making/Breaking upon Electron Transfer. *Angew. Chem. Int. Ed.* **2001**, *40* (17), 3251–3254. https://doi.org/10.1002/1521-3773(20010903)40:17<3251::AID-ANIE3251>3,0.CO;2-P.
- (37) Suzuki, T.; Ishigaki, Y.; Iwai, T.; Kawai, H.; Fujiwara, K.; Ikeda, H.; Kano, Y.; Mizuno, K. Multi-Input/Multi-Output Molecular Response System Based on the Dynamic Redox Behavior of 3,3,4,4-Tetraaryldihydro[5]Helicene Derivatives: Reversible Formation/Destruction of Chiral Fluorophore and Modulation of Chiroptical

- Properties by Solvent Polarity. *Chem. Eur. J.* **2009**, *15* (37), 9434–9441. https://doi.org/10.1002/chem.200900968.
- (38) Schweinfurth, D.; Zalibera, M.; Kathan, M.; Shen, C.; Mazzolini, M.; Trapp, N.; Crassous, J.; Gescheidt, G.; Diederich, F. Helicene Quinones: Redox-Triggered Chiroptical Switching and Chiral Recognition of the Semiquinone Radical Anion Lithium Salt by Electron Nuclear Double Resonance Spectroscopy. *J. Am. Chem. Soc.* **2014**, *136* (37), 13045–13052. https://doi.org/10.1021/ja5069323.
- (39) Tamaoki, H.; Katoono, R.; Fujiwara, K.; Suzuki, T. Assembly of an Axially Chiral Dynamic Redox System with a Perfluorobiphenyl Skeleton into Dumbbell- or Tripod-Type Electron Donors. *Angew. Chem. Int. Ed.* **2016**, *55* (7), 2582–2586. https://doi.org/10.1002/anie.201510935.
- (40) Jin, Z.; Cheng, Q.; Bao, S. T.; Zhang, R.; Evans, A. M.; Ng, F.; Xu, Y.; Steigerwald, M. L.; McDermott, A. E.; Yang, Y.; Nuckolls, C. Iterative Synthesis of Contorted Macromolecular Ladders for Fast-Charging and Long-Life Lithium Batteries. *J. Am. Chem. Soc.* **2022**, *144* (30), 13973–13980. https://doi.org/10.1021/jacs.2c06527.
- (41) de Leeuw, D. M.; Simenon, M. M. J.; Brown, A. R.; Einerhand, R. E. F. Stability of N-Type Doped Conducting Polymers and Consequences for Polymeric Microelectronic Devices. *Synth. Met.* **1997**, *87* (1), 53–59. https://doi.org/10.1016/S0379-6779(97)80097-5.
- (42) Sharma, V.; Puthumana, U.; Karak, P.; Koner, A. L. Visible-Light-Triggered Generation of Ultrastable Radical Anion from Nitro-Substituted Perylenediimides. *J. Org. Chem.* **2018**, *83* (18), 11458–11462. https://doi.org/10.1021/acs.joc.8b02023.
- (43) We Acknowledge That Due to the Intrinsic Error of the Chirascan V100 Spectropolarimeter above 800 Nm That the True Value for the  $|g_{abs}|$  May Be Overestimated.
- (44) Shen, C.; Loas, G.; Srebro-Hooper, M.; Vanthuyne, N.; Toupet, L.; Cador, O.; Paul, F.; López Navarrete, J. T.; Ramírez, F. J.; Nieto-Ortega, B.; Casado, J.; Autschbach, J.; Vallet, M.; Crassous, J. Iron Alkynyl Helicenes: Redox-Triggered Chiroptical Tuning in the IR and Near-IR Spectral Regions and Suitable for Telecommunications Applications. *Angew. Chem.* **2016**, *128* (28), 8194–8198. https://doi.org/10.1002/ange.201601633.
- (45) Shen, C.; He, X.; Toupet, L.; Norel, L.; Rigaut, S.; Crassous, J. Dual Redox and Optical Control of Chiroptical Activity in Photochromic Dithienylethenes Decorated with Hexahelicene and Bis-Ethynyl-Ruthenium Units. *Organometallics* **2018**, *37* (5), 697–705. https://doi.org/10.1021/acs.organomet.7b00534.
- (46) Medel, M. A.; Hortigüela, L.; Lloveras, V.; Catalán-Toledo, J.; Miguel, D.; Mota, A. J.; Crivillers, N.; Campaña, A. G.; Morcillo, S. P. N-Doped Octagon-Containing HBC as Redox and pH Chiroptical Switch in the NIR. *ChemistryEurope n/a* (n/a), e202300021. https://doi.org/10.1002/ceur.202300021.
- (47) Wan, L.; Zhang, R.; Cho, E.; Li, H.; Coropceanu, V.; Brédas, J.-L.; Gao, F. Sensitive Near-Infrared Circularly Polarized Light Detection via Non-Fullerene Acceptor Blends. *Nat. Photonics* **2023**, *17* (8), 649–655. https://doi.org/10.1038/s41566-023-01230-z.
- (48) Hong, G.; Antaris, A. L.; Dai, H. Near-Infrared Fluorophores for Biomedical Imaging. *Nat. Biomed. Eng.* **2017**, *1* (1), 1–22. https://doi.org/10.1038/s41551-016-0010.
- (49) Connelly, N. G.; Geiger, W. E. Chemical Redox Agents for Organometallic Chemistry. *Chem. Rev.* **1996**, *96* (2), 877–910. https://doi.org/10.1021/cr940053x.
- (50) Martin, R. L. Natural Transition Orbitals. J. Chem. Phys. 2003, 118 (11), 4775–4777. https://doi.org/10.1063/1.1558471.
- (51) Lu, T.; Chen, F. Multiwfn: A Multifunctional Wavefunction Analyzer. *J. Comput. Chem.* **2012**, *33* (5), 580–592. https://doi.org/10.1002/jcc.22885.

# Insert Table of Contents artwork here

#